Vibrational Spectroscopy 97 (2018) 135–139

Contents lists available at ScienceDirect

Vibrational Spectroscopy

journal homepage: www.elsevier.com/locate/vibspec

Vibrational spectra calculation of squamous cell carcinoma in the amide band region

Daiana R. Bortoletto[a], Cassio A. Lima[b], Denise Zezell[b], Erika T. Sato[a], H. Martinho[a,*]

[a] Centro de Ciências Naturais e Humanas, Universidade Federal do ABC, Av. dos Estados 5001, Santo André, SP 09210-580, Brazil
[b] Center for Lasers and Applications, Instituto de Pesquisas Energéticas e Nucleares, IPEN-CNEN/SP, São Paulo, SP 05508-000, Brazil

ARTICLE INFO

Keywords:
Squamous cell carcinoma
Optical biopsy
Vibrational spectroscopy
FTIR
Skin cancer
Density Functional Theory
Computational simulation
Tissue computer model

ABSTRACT

Alterations in the amide (1500–1700 cm^{-1}) spectral region probed by Fourier-transform infrared spectroscopy (FTIR) have been reported comparing tumor and normal tissues. Usually, bands in this range are assigned to the so-called Amide I, II, and III vibrations which provide pieces of information concerning peptide bonds and secondary structure (α-helix, β-sheet) of proteins. Proteins folding changes due to tumoral process are usually considered to qualitatively explain the observed differences between tumor and normal tissues. In this paper, the observed changes in the FTIR spectra of squamous cell carcinoma compared to normal tissues were analyzed by First-Principles Density Functional Theory vibrational calculations. Computational models for skin and prototype β-sheet model were employed. Our findings shown that predominates conjugated Amide I + Amide II, Amide V, methylene torsions, and ring side chains torsions and swings vibrations in this region. We also notice the lack of evidence concerning changes in the secondary structure of the β-sheet peptidic model to explain the spectral differences. In fact, we concluded that the proline amino acid has the main rule to explain the data in this region being it responsible for the strong coupling between vibrations instead of water.

1. Introduction

More than 20 million new cases of cancer are estimated for 2025 in developing countries in part influenced by a growing global population and by aging [1]. This demands special attention from the public healthy authorities.

Tumors that develop from the epithelial cells such as epithelial cells lining the skin that form the protective cellular layers are known as squamous cell carcinomas [2]. Skin cancer is the most frequent in all populations, presenting in two forms: melanoma and nonmelanoma. The former is the most aggressive form of skin cancer. It consists of a malignant proliferation of melanocytes, which are the pigmented cells of the skin, and occur less frequently. Nonmelanoma skin cancers (NMSC) are neoplasms with a good prognosis and high cure rates. The incidence of both skin cancers, melanoma and nonmelanoma, has increased over the decades. Between 2 and 3 million NMSC and 132,000 melanomas occur globally each year. One in three diagnosed cancers is a skin cancer according to Skin Cancer Foundation Statistics [3]. SCC is one of the main forms of NMSC. It is responsible for 25% of diagnoses, aggressive, invasive, destructive and metastatic growth pattern [4–6].

When detected early, the treatment of cancer can be successful. The actual gold standard method for discrimination of normal and altered tissues is the histopathological analysis performed on a biopsied tissue. Considerable time and costs are required to obtain the biopsy, and the specialized knowledge of a pathologist is necessary for the diagnosis. However, the available screening and diagnostic methods have their failures. New diagnostic tools based on photonic technology have been developed to achieve treatment with favorable results. One of these tools is the optical biopsy. Optical biopsy refers to techniques where the light-tissue interaction is analyzed and the tissue state information is obtained both “in vivo” and “ex vivo”. Biological materials had been successfully characterized using these kinds of techniques. Vibrational spectroscopy, consisting of Raman scattering and Fourier-transform infrared (FTIR) techniques, are of particular interest due of their high sensitivity in the detection of biochemical and molecular changes in biological tissues [7–11]. They have been considered as promising techniques for the detection of cancer due to its advantages over conventional diagnostic methods: absence of tissue removal, minimally invasive character, and reproducibility [12]. The characteristics of molecular interactions in cells and tissues, which cannot be directly accessed by conventional histopathology, can be accessed by FTIR. In particular, the vibrational modes associated with important biochemical components of cells can be used as markers in the identification of metabolic alterations suffered by the cell during the carcinogenesis

* Corresponding author.
E-mail address: herculano.martinho@ufabc.edu.br (H. Martinho).

https://doi.org/10.1016/j.vibspec.2018.06.007
Received 19 April 2018; Received in revised form 28 May 2018; Accepted 12 June 2018
Available online 20 June 2018
0924-2031/

process. For this, more studies are demanded to better understand how biochemical changes translate into structural changes that lead to these pathological conditions.

Significant alterations in the so-called Amide I, II and III bands (1500–1700 cm^{-1}) have been reported when comparing tumor and normal tissues, providing information on vibrational modes from peptide bonds and secondary structure of proteins [13–15]. The band at ~1517 cm^{-1} (Amide II) results from the out of phase combination of N−H flexion in the plane and C−N stretching with small contributions of C═O flexion in the plane and C−C and N−C stretches of peptide bonds [16,13]. The bands at ~1638 cm^{-1} [17], ~1655 cm^{-1} [16,17] and ~1694 cm^{-1} [16,17] (Amide I) are characterized by C═O stretching with small contributions of out of phase C−N stretch, C−C−N deformation and N−H flexion in the plane [13]. The ~1638 cm^{-1} and ~1694 cm^{-1} bands are usually associated with the parallel and anti-parallel configuration of the secondary β-sheet structure of proteins, respectively. These bands have been frequently recognized as markers of the peptide and protein secondary structure [13]. Since Amide II vibrational band is hardly affected by the side-chain vibrations, the correlation between secondary structure and its frequency is less straightforward than that for Amide I bands [18].

In particular, Lima et al. [14] reported that sub-bands of Amide I related to α-helix (1655 cm^{-1}) and parallel β-sheet (1638 cm^{-1}) structures of proteins showed a higher intensity increase and shifted in SCC tissue compared to normal skin. Parallel β-sheet shifted 4 cm^{-1} to a lower wavenumbers, whereas a shift of 2 cm^{-1} to higher wavenumber was found for the α-helix structure. The authors suggested that changes in hydrogen bonding between peptide groups and consequently in molecular geometry of proteins may induce damages in protein folding resulting in loss of protein biological function or mutation.

Since the tissue vibrational bands assignment is usually made based on isolated macromolecules assignment, anharmonic interactions which gives rise to a coupling among harmonic modes and mutual interactions among specific moieties as well are considered on a qualitative basis.

Computational simulations are widely used to study and make predictions about a large variety of systems ranging from pharmacology to engineering fields [19–21]. Atomistic models based on quantum mechanics calculations have better predictability in the material properties. However, due to its inherent complexity, atomistic models for biological tissues are absent in the literature. These models would be useful for understanding the physical and biochemical properties of tissues. Computational simulations could be used as a tool to better understand how biochemical changes translate into structural changes that generate pathological states. By computational calculations, it is possible to obtain the vibrational spectrum of molecules and macromolecules. It is possible to verify which atoms or molecules contribute to the existence of each characteristic vibrational mode, identify and interpret the interactions between these modes, and associate these pieces of information to the pathological processes.

In a previous work [22] of our research group we presented a computational model for skin (STmod). The model consisted of a collagen peptide cutout including confined water submitted to periodic boundary conditions. Using that model we successfully explained important experimental structural and general biochemical trends of normal and inflammatory tissues.

In the present work we present a sophisticated version of our STmod model built to consider SCC characteristics. We calculated the detailed FTIR vibrational modes by First-Principles Density Functional Theory (DFT) in the Amide (1500–1700 cm^{-1}) region. Comparisons with normal and SCC tissues experimental data and β-sheet model were also performed.

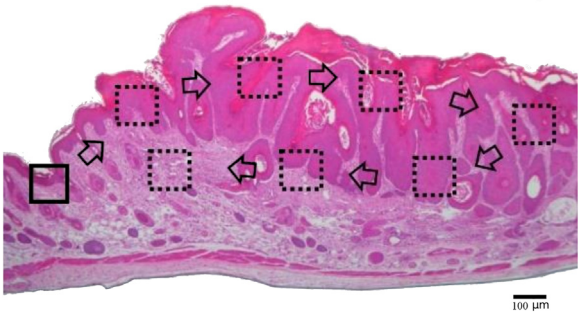

Fig. 1. Light microscopy (10×) of representative histological sections hematoxylin–eosin (H&E) stained of SCC lesion. FTIR spectra where acquired in the sites indicated by squares.

2. Methodology

2.1. Experimental

Cutaneous neoplastic lesions (SCC) were chemically induced on Swiss mice using a well-established multi-stage chemical carcinogenesis protocol [14,24]. Healthy (NM) and diseased tissues were obtained by excisional necropsies, formalin-fixed for 24 h and paraffin-embedded. Longitudinal sections with 5-µm thickness were placed on MirrIR low-E-coated slides (Kevley Technologies) and submitted to dewaxing protocol prior the spectroscopic measurements. Spectra where collected on 8–10 different sites in each histological slice (see Fig. 1). Predominates the sampling on dermis region. Infrared absorption spectra in the fingerprint region (900–1800 cm^{-1}) for these tissues were obtained with the Thermo Nicolet 6700 FTIR spectrometer (Thermo Scientific) coupled to a Smart Orbit attenuated reflection accessory (Thermo Scientific). See Ref. [14] for more details.

2.2. Computational model

We used the STmod for normal skin [22] as starting point. In the real soft connective tissue, larger fibrillar bundles are formed by different types of collagen. These fibers are formed by semi-crystalline aggregates of collagen molecules formed by twisted peptides, with more than 1000 amino acids in each and the presence of water between the structures. Under periodic contour conditions, the model simulates the dermis tissue representing the fibrils and the presence of water between them. In the dimensional scale of the model, the collagen fibrils were associated to a reticulated set of unit cells whose internal constitution was chosen by the water molecules present there. In this approach the tissue complexity was replaced by this periodic set, using periodic boundary conditions. The vibrational calculations were performed on C_n (n − 8), C_{1s}, D_0, D_1 unit cells of STmod, and a β-sheet structure prototype (2n6h structure from Protein Data Bank [23]). The numeric subscript in STmod indicates the number of water molecules inside the unit cell. The “s” subscript related to the presence of external water solvating the C_1 model. Starting from a hydrated collagen peptide each unit cell was obtained and calculations performed on periodic boundary conditions. More details concerning the obtainment of these structures and previous characterizations as well could be found in Ref. [22].

Fig. 2 shows the unit cell for C_0, C_1, C_2, D_1, and β-sheet structures. Density Functional Theory (DFT)[25,26] was used in order to obtain the equilibrium geometries and harmonic frequencies. The simulations were implemented in the CPMD program [27] using the BLYP functional [28] augmented with dispersion corrections for the proper description of van der Waals interactions [29,30]. The cutoff energy was 100 Ry. The wave functions were optimized and then the vibrational modes were obtained using the Hessian matrix. Finally the linear response for the values of polarization and polar tensors of each atom in the system was calculated to evaluate the eigenvectors of each

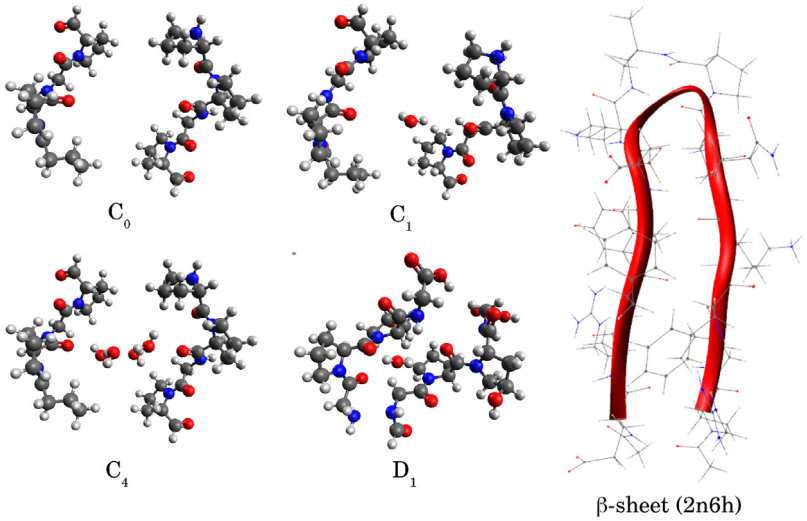

Fig. 2. Unit cells for C_0, C_1, C_4, D_1, and β-sheet (2n6h) [23].

vibrational mode. Experimental data were compared to the vibrational calculations performed on all models. For experimental data comparison, the calculated spectra were simulated as a convolution of Gaussian lineshape peaks centered on the calculated frequencies using the Fityk [31] program. The linewidth was chosen to be 20 cm^{-1}. The analysis of the vibrations was done using the archives constructed with the atomic polar tensor for visualization of the vibrational modes, so that it is possible to make a complete and detailed analysis of the assignments of each band.

3. Results and discussion

The normalized and baseline corrected experimental average FTIR data for NM and SCC tissues are shown in Fig. 3.

The experimental spectra of the NM and SCC tissues; the simulated spectra of C_n (n − 8), C_{1s}, D_0, D_1 models; and the simulated spectra of β-sheet prototype are represented in Fig. 4a in the Amide region (1500–1700 cm^{-1}). Computing the first-derivative of the difference spectra among NM and SCC it was possible to discern those regions of relevant spectral differences among the data (Fig. 4b). Considering points of zero, maximum or minimum of derivative it was found five frequencies with important differences between groups: 1515 cm^{-1}, 1558 cm^{-1}, 1582 cm^{-1}, 1605 cm^{-1} and 1655 cm^{-1} (arrows in Fig. 4b). The derivative around 1640 cm^{-1} presented an oscillatory behavior. Since this band was used to normalize the data it was not

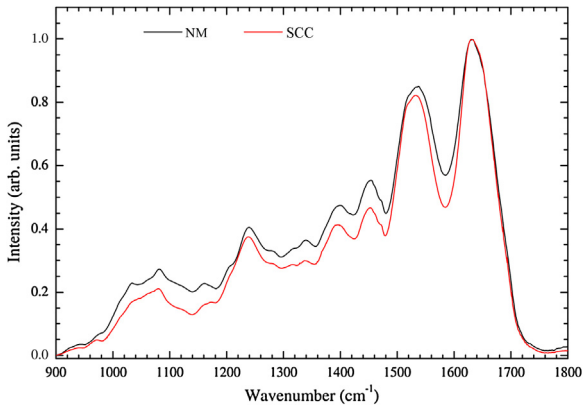

Fig. 3. Experimental data of normal (NM, black line) and neoplastic (SCC, red line) tissues. (For interpretation of the references to color in this figure legend, the reader is referred to the web version of the article.)

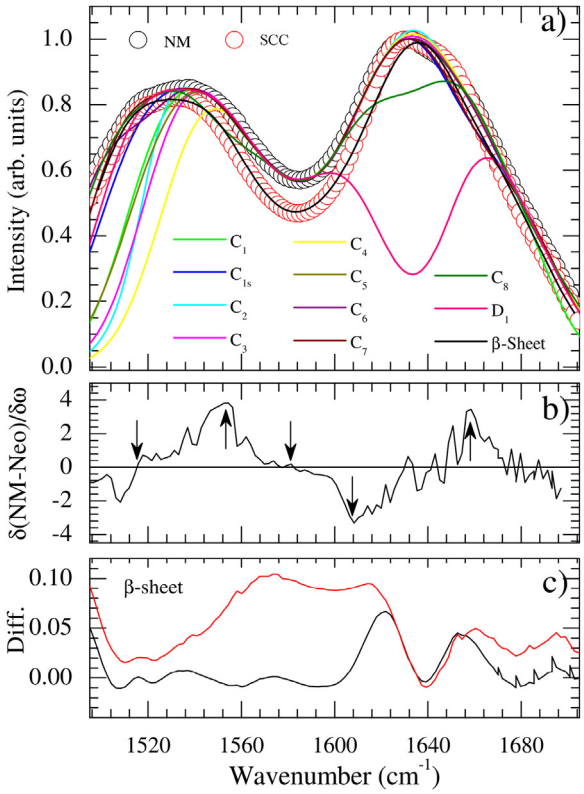

Fig. 4. (a)FT-IR experimental data for normal (NM) and neoplastic (SCC) tissues and simulations using the vibrational calculations of models of skin C_n (n − 8), C_{1s}, D_0, D_1 and β-sheet as well. (b) First-derivative of the difference plot between NM and SCC experimental data. Arrows indicate points of significant differences. (c) Difference between experimental data and simulated β-sheet model (black line: NM, red line: SCC). (For interpretation of the references to color in this figure legend, the reader is referred to the web version of the article.)

considered in our analysis.

The above-mentioned five frequencies were compared with the calculated vibrations searching for similarities. It was found that the 1515 cm^{-1} frequency is present in the C_7, C_8 and D_1 models. The only model presenting vibration around 1558 cm^{-1} was the C_8 one. The frequency 1605 cm^{-1} was present in the C_{1s} model. The 1655 cm^{-1} mode was present on C_1–C_8 models. The frequency 1582 cm^{-1} was not

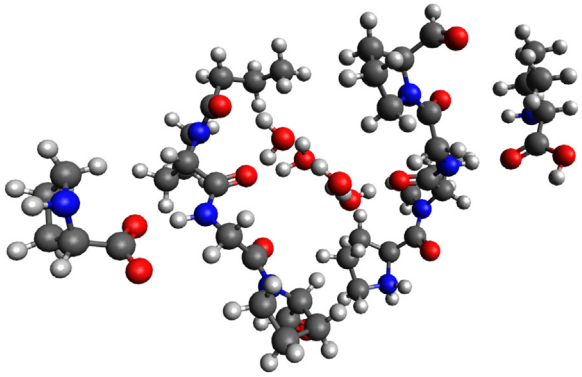

Fig. 5. Unit cell of the C_4PV model. This model corresponds to the C_4 one including proline and valine amino acids in specific *loci*.

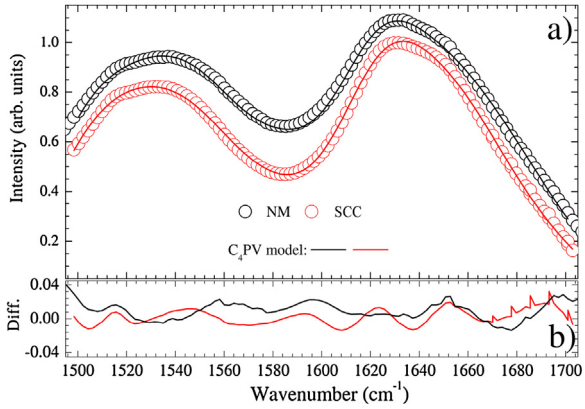

Fig. 6. (a)FT-IR experimental data for normal (NM) and neoplastic (SCC) tissues and simulations using the vibrational calculations of C_4PV model. NM data were vertically translated by 0.2 for better visualization. (b) Difference between experimental data and simulated C_4PV model (black line: NM, red line: SCC). (For interpretation of the references to color in this figure legend, the reader is referred to the web version of the article.)

explained by any of the computational models. The C_4 model was able to describe almost all bands, except the 1515 cm^{-1} one. The β-sheet model displayed all bands in this region. Fig. 4c shows the difference between experimental data and β-sheet model simulated spectra (black line: NM, red line: SCC). The β-sheet model presented a better agreement for NM case.

Raman spectroscopy studies performed by Gniadecka et al. [32] found an increased amount of the non-macromolecule bound, tetrahedral water in photo-aged and malignant tumors of the skin compared to normal tissues. Computational simulations performed by Sato et al. [22] also recognized the important role of tetrahedral water cluster on inflammatory infiltrates. Bearing it in mind, it was tested the viability of expand the C_4 model incorporating specific moieties in order to explain SCC experimental data.

3.1. C_4PV model

Gniadecka et al. [32] presented one of the first reports concerning BCC diagnosis by Raman spectroscopy using the 800–1000 cm^{-1} region. They find important differences between normal skin and BCC tumor tissues. They attributed the observed difference to stretching vibrations of simple bonds for the amino acids proline and valine and polysaccharides as well. In fact, it has been recognized that proline develops important functions in tumorigenesis, linking the reprogramming of glucose, glutamine and pyridine nucleotides [33], apoptosis, autophagy and in response to nutrient and oxygen deprivation [33]. Proline-derived reactive oxygen species served as a driving signal for reprogramming [33]. Thus, we tested an improved version of the C_4 model which includes proline and valine amino acids (labeled as C_4PV model) which would best describes the tumor experimental data. Fig. 5 shows the orthorhombic unit cell of the C_4PV model with dimension a = 22, 158Å, b = 12, 617Å, and c = 14, 018Å. The harmonic frequencies generated in the computational simulation of the C_4PV model were compared with experimental data of FTIR spectroscopy for SCC, as shown in Fig. 6a. The simulation procedure followed the above-mentioned steps. The accordance between experimental and simulated data was remarkable. Fig. 6b shows the difference among experimental data and C_4PV model simulated spectra (black line: NM, red line: SCC). The maximum observed difference was of ~0.01 for NM and SCC being its two orders of magnitude smaller than the β-sheet model (Fig. 4c).

The assignment of vibrational modes based on C_4PV model can be found in Table 1. Predominates conjugated Amide I + Amide II, Amide V, methylene torsions, and ring side chains torsions and swings vibrations. It is noticed that confined water plays no role in this spectral region. The protonated proline is the responsible for the strong coupling between vibrations instead of water.

4. Conclusions

It is important to mention that the computational model considered is a general representation of the dermis. It excludes dermis constituents as mechanoreceptors, thermoreceptors, glands, follicles, vessels, and fibrillar matrix as well [34]. In spite of this the results show that the C_4PV model presents an excellent description of the FTIR experimental data. This fact indicates that absorption of infrared radiation by amino acids of the skin is the main light-tissue interaction process in the fingerprint region (800–1800 cm^{-1}).

The β-sheet model, usually evoked to explain spectral changes in tumor tissues in the Amide region, did not reproduce the vibrational spectrum of SCC at similar level of agreement as C_4PV one. No evidence for changes in the secondary structure of the β-sheet peptidic model was

Table 1
Assignment altered vibrational modes on neoplastic tissue (SCC) compared to the normal one (see Fig. 4b) based on C_4PV model. The usual assignment based on literature (Movasaghi et al. [16]) is also given.

Exp. (cm^{-1})	Simul. (cm^{-1})	Usual assign	Our assign
1515	1520	Amide II	Amide II, conjugated Amide I – Amide II vibration; Amide V; intense CH_2 torsion; asymmetric torsion of CH_2; CH_2 asymmetric torsion (ring); CH_2 swing (ring); NH_2 torsion (ring); CH_2 rotation (ring).
1558	1557	Ring base	(vibrations of functional groups closer to proline) Amide II; Amide V; asymmetric scissors of C-O-H; CH_2 swing (ring); C—N stretching (ring);CH_2 asymmetric torsion (ring).
1582	1584	Ring C—C stretch of phenyl	(vibrations of functional groups closer to proline) Amide II; conjugated Amide I – Amide II vibration; Amide V; asymmetric torsion of CH_2 (proline); asymmetric torsion C—H—O;CH_2 swing (ring); C—H asymmetric torsion (ring).
1605	1602	ν (COO^-) (polysaccharides, pectin)	CH_2 torsion and rotation in proline; conjugated Amide I - Amide II vibration; Amide II; Amide V; CH_2 rotation and torsion (ring); torsion NH_2 (ring).
1655	1661	Amide I	(vibrations of functional groups closer to proline) Amide I; conjugated Amide I – Amide II vibration; Amide V; CH_2 torsion; CH_2 swing and torsion with angular folding (ring).

found to explain the SCC and NM spectral differences. However, for NM tissue, there is relative agreement between the two models, being the difference between experimental and simulated data $\lesssim 0.05$ (Figs. 4c and 6b). Notwithstanding the confined water relevance in the tumor pathology in the Amides region the proline amino has the main role with corroborates independent experimental findings concerning its relevance in tumorogenesis.

Acknowledgements

The authors would like to thank the Brazilian agencies Conselho Nacional de Desenvolvimento Científico e Tecnológico (CNPq – 311146/2015-5) and Fundação de Amparo à Pesquisa do Estado de São Paulo (FAPESP – 2011/19924-2) for the financial support. The authors would also thank the computational resources provided by Centro Nacional de Processamento de Alto Desempenho em São Paulo (CENAPAD-UNICAMP) and Sistema de Computação Petaflópica (Tier 0) (Santos Dumont-LNCC) under Sistema Nacional de Processamento de Alto Desempenho (SINAPAD) of the Ministério da Ciência, Tecnologia e Inovação (MCTI).

References

[1] B.W. Stewart, C.P. Wild, World cancer report 2014, (2014).
[2] R. Weinberg, The Biology of Cancer, Garland Science, 2013.
[3] P. Boyle, B. Levin, World cancer report 2008, (2008).
[4] L.E. Dubas, A. Ingraffea, Nonmelanoma skin cancer, Facial Plast. Surg. Clin. 21 (2013) 43–53.
[5] R. Kim, A. Armstrong, Nonmelanoma skin cancer, Dermatol. Clin. 30 (2012) 125–139.
[6] D.A. Lee, S.J. Miller, Nonmelanoma skin cancer, Facial Plast. Surg. Clin. 17 (2009) 309–324 Skin Cancer..
[7] M. Diem, A. Mazur, K. Lenau, J. Schubert, B. Bird, M. Miljkovic, C. Krafft, J. Popp, Molecular pathology via IR and Raman spectral imaging, J. Biophotonics 6 (2013) 855–886.
[8] M. Diem, M. Miljkovi, B. Bird, T. Chernenko, J. Schubert, E. Marcsisin, A. Mazur, E. Kingston, E. Zuser, K. Papamarkakis, N. Laver, Applications of infrared and Raman microspectroscopy of cells and tissue in medical diagnostics: present status and future promises, Spectrosc. Int. J. 27 (2012).
[9] M. Diem, P. Griffiths, J. Chalmers, Vibrational Spectroscopy for Medical Diagnosis, John Wiley & Sons, Inc, New Jersey, USA, 2008.
[10] M.J. Baker, J. Trevisan, P. Bassan, R. Bhargava, H.J. Butler, K.M. Dorling, P.R. Fielden, S.W. Fogarty, N.J. Fullwood, K.A. Heys, et al., Using Fourier transform IR spectroscopy to analyze biological materials, Nat. Protoc. 9 (2014) 1771–1791.
[11] H.J. Byrne, M. Baranska, G.J. Puppels, N. Stone, B. Wood, K.M. Gough, P. Lasch, P. Heraud, J. Sule-Suso, G.D. Sockalingum, Spectropathology for the next generation: quo vadis? Analyst 140 (2015) 2066–2073.
[12] H. Martinho, Cancer – Cares, Treatments and Preventions, iConcept Press Ltd., 2014, pp. 255–280.
[13] A. Barth, Infrared spectroscopy of proteins, Biochim. Biophys. Acta (BBA) – Bioenergetics 1767 (2007) 1073–1101.
[14] C.A. Lima, V.P. Goulart, L. Côrrea, T.M. Pereira, D.M. Zezell, ATR-FTIR spectroscopy for the assessment of biochemical changes in skin due to cutaneous squamous cell carcinoma, Int. J. Mol. Sci. 16 (2015) 6621–6630.
[15] S. De Bruyne, M.M. Speeckaert, J.R. Delanghe, Applications of mid-infrared spectroscopy in the clinical laboratory setting, Crit. Rev. Clin. Lab. Sci. (2017) 1–20.
[16] Z. Movasaghi, S. Rehman, I.U. Rehman, Fourier transform infrared (FTIR)spectroscopy of biological tissues, Appl. Spectrosc. Rev. 43 (2008) 134–179.
[17] R. Khurana, A.L. Fink, Do parallel beta-helix proteins have a unique Fourier transform infrared spectrum? Biophys. J. 78 (2000) 994–1000.
[18] S. Olsztynska-Janus, A. Pietruszka, Z. Kielbowicz, M. Czarnecki, ATR-IR study of skin components: lipids, proteins and water. Part I: temperature effect, Spectrochim. Acta A 188 (2018) 37–49.
[19] L. Xie, L. Xie, S.L. Kinnings, P.E. Bourne, Novel computational approaches to polypharmacology as a means to define responses to individual drugs, Annu. Rev. Pharmacol. Toxicol. 52 (2012) 361–379.
[20] M.O. Steinhauser, S. Hiermaier, A review of computational methods in materials science: examples from shock-wave and polymer physics, Int. J. Mol. Sci. 10 (2009) 5135.
[21] A. Yazid, N. Abdelkader, H. Abdelmadjid, A state-of-the-art review of the X-FEM for computational fracture mechanics, Appl. Math. Model. 33 (2009) 4269–4282.
[22] E.T. Sato, A.R. Rocha, L.F.d.C.e.S. de Carvalho, J.D. Almeida, H. Martinho, Molecular model for hydrated biological tissues, Phys. Rev. E 91 (2015) 063310.
[23] V.M. Kung, G. Cornilescu, S.H. Gellman, Impact of strand number on parallel β-sheet stability, Angew. Chem. Int. Ed. 54 (2015) 14336–14339.
[24] E.L. Abel, J.M. Angel, K. Kiguchi, J. DiGiovanni, Multi-stage chemical carcinogenesis in mouse skin: fundamentals and applications, Nat. Protoc. 4 (2009) 1350.
[25] P. Hohenberg, W. Kohn, Inhomogeneous electron gas, Phys. Rev. 136 (1964) B864–B871.
[26] W. Kohn, L.J. Sham, Self-consistent equations including exchange and correlation effects, Phys. Rev. 140 (1965) A1133–A1138.
[27] Cpmd, http://www.cpmd.org/,copyright ibm corp 1990–2008, copyright mpi für festkörperforschung stuttgart., 1997–2001.
[28] C. Lee, W. Yang, R.G. Parr, Development of the Colle-Salvetti correlation-energy formula into a functional of the electron density, Phys. Rev. B 37 (1988) 785.
[29] O.A. von Lilienfeld, I. Tavernelli, U. Rothlisberger, D. Sebastiani, Performance of optimized atom-centered potentials for weakly bonded systems using density functional theory, Phys. Rev. B 71 (2005) 195119.
[30] I.-C. Lin, M.D. Coutinho-Neto, C. Felsenheimer, O.A. von Lilienfeld, I. Tavernelli, U. Rothlisberger, Library of dispersion-corrected atom-centered potentials for generalized gradient approximation functionals: elements H, C, N, O, He, Ne, Ar, and Kr, Phys. Rev. B 75 (2007) 205131.
[31] Fityk. y(x) curve fitting and data analysis, 2009.
[32] M. Gniadecka, H. Wulf, N.N. Mortensen, O.F. Nielsen, D.H. Christensen, Diagnosis of basal cell carcinoma by Raman spectroscopy, J. Raman Spectrosc. 28 (1997) 125–129.
[33] W. Liu, C.N. Hancock, J.W. Fischer, M. Harman, J.M. Phang, Proline biosynthesis augments tumor cell growth and aerobic glycolysis: involvement of pyridine nucleotides, Sci. Rep. 5 (2015).
[34] J.G. Marks, J.J. Miller, Lookingbill and Marks' Principles of Dermatology E-Book, Elsevier Health Sciences, 2017.